Form birefringence in UV-exposed photosensitive fibers computed using a higher order finite element method

N. Belhadj and S. LaRochelle

Centre d'Optique, Photonique et Laser (COPL), Département de génie électrique et de génie informatique, Université Laval, (Québec) Canada G1K 7P4,
larochel@gel.ulaval.ca

K. Dossou

Département de mathématiques et de statistique, Université Laval, (Québec) Canada G1K 7P4

Abstract: The effective index change and form birefringence are calculated in UV-exposed fibers using a high-order vectorial finite element method. The birefringence is compared in optical fibers with and without photosensitive inner cladding.

OCIS codes: (060.0060) Fiber optics and optical communications, (060.2340) fiber optics components, (060.2430) fibers single-mode.

References

1. R. Gafsi, and M. A. El-Sherif, ''Analysis of Induced-Birefringence Effects on Fiber Bragg Gratings,'' Opt. Fiber Technol. **6**, 299-323 (2000).
2. T. Erdogan, and V. Mizrahi, ''Characterization of UV-induced birefringence in photosensitive Ge-doped silica optical fibers,'' J. Opt. Soc. Am. **B 11**, 2100-2105 (1994).
3. D. Innis, Q. Zhong, A. M. Vengserkar, W. A. Reed, S. G. Kosinski, and P. J. Lemaire, ''Atomic force microscopy study of uv-induced anisotropy in hydrogen-loaded germanosilicate fibers,'' Appl. Phys. Lett. **65**, 1528-1530 (1994).
4. A. M. Vengsarkar, Q. Zhong, D. Innis, W. A. Reed, P. J. Lemaire, and S. G. Kosinski ''Birefringence reduction in side-written photoinduced fiber devices by a dual-exposure method,'' Opt. Lett. **19**, 1260-1262 (1994).
5. H. Renner, ''Effective index increase, form birefringence and transmission losses in UV-illuminated photosensitive fiber,'' Opt. Express **9**, 546-560 (2001) http://www.opticsexpress.org/abstract.cfm?URI=OPEX-9-11-546 .
6. K. Dossou, S. LaRochelle, and M. Fontaine, ''Numerical Analysis of the Contribution of the transverse asymmetry in the photo-induced index change profile to the birefringence of optical fiber,'' J. Lightwave Technol. **20**, 1463-1469 (2002).
7. N. Belhadj, K. Dossou, X. Daxhelet, S. LaRochelle, S. Lacroix, and M. Fontaine, ''A comparative study of numerical methods for the calculation of the birefringence of UV-illuminated fibers'', OSA Technical Digest : Conference on Bragg Gratings, Photosensitivity and Poling in Glass Waveguides, Monterey, California, USA, September 1-3, (paper MD20) 112-114 (2003).
8. L. Dong, G. Qi, M. Marro, V. Bhatia, L. L. Hepburn, M. Swan, A. Collier, and D. L. Weidman ''Suppression of Cladding Mode Coupling Loss in Fiber Bragg Gratings,'' J. Lightwave Technol. **18**, 1583-1590 (2000).
9. L. Dong, W. H. Loh, J.E. Caplen, and J.D. Minelly, ''Efficient single-frequency fiber lasers with novel photosensitive Er/Yb optical fibers,''Opt. Lett. **22**, 694-696 (1997).
10. K. Dossou, Département de mathématique et de statistique, Université Laval, (Québec) Canada G1K 7P4, and M. Fontaine are preparing a manuscript to be called "A high order isoparametric finite element method for computation of waveguide modes."
11. H. Patrick and S. L. Gilbert, "Growth of Bragg gratings produced by continuous-wave ultraviolet light in Optical fiber", Opt. Lett. **18**, 1484-1486 (1993).
12. M. Koshiba, S. Maruyama, and K. Hirayama, ''A Vector Finite Element Method with the high-order mixed-interpolation-type triangular elements for optical waveguiding problems,'' J. Lightwave Technol. **12**, 495-502(1994).

#4024 - $15.00 US Received 16 March 2004; revised 6 April 2004; accepted 6 April 2004

13. L. Demkowicz, and L. Vardapetyan, ''Modeling of electromagnetic absorption/scattering problems using hp-adaptive finite elements,'' Comput. Methods Appl. Mech. Engrg. **152**, 103-124 (1998).

1. Introduction

Photo-induced birefringence is an important concern in the fabrication of fiber Bragg grating based components. Previous studies have identified three contributions to the photo-induced birefringence of gratings: the photo-induced stress due to the glass structure densification in the photosensitive core fiber [1], the orientation of the writing beam polarization [2] and the asymmetries of the index change profile in the transverse plane called form birefringence [3,4]. The form birefringence results from the absorption of the UV beam in the transverse plane of the fiber due to the one-side illumination. The asymmetry of the refractive index profile was observed using an atomic force microscopy [3] and the contribution from the form birefringence to the UV-induced birefringence was investigated and reduced by Vengsarkar et al. using dual exposure of the fiber [4]. Recently, the birefringence resulting from the transverse asymmetry of the index profile in UV-exposed fibers has been calculated using different numerical methods [5,6]. Vectorial and scalar numerical methods were compared for the calculation of the effective index and the form birefringence [7]. Under the assumption of an exponential decay of the index change across the core, a quasi-quadratic dependence of the birefringence on the effective index variation is predicted by all methods. In all cases, the form birefringence is estimated to be smaller than $1x10^{-5}$ for effective index change lower than $3x10^{-3}$ [7]. The full vectorial formulation with high order interpolation polynomials of the vectorial finite element method (VFEM) and the finite difference method with polarization correction were found to give almost identical results of the computed form birefringence [7]. All calculations were performed considering standard single-mode fiber with a photosensitive core. However, photosensitive specialty optical fibers are often manufactured with a photosensitive core and a photosensitive inner cladding to suppress unwanted coupling to cladding modes [8]. Other fibers, used in the fabrication of distributed-feedback fiber lasers, are manufactured without photosensitivity in the core in order to separate the photosensitive region, with high germanium concentration, from the erbium/ytterbium co-doped core. This fiber design reduces clustering of the Er ions in the highly-doped fiber core [9]. In this paper, we examine, through numerical calculations, the impact of the presence of a photosensitive cladding on the birefringence resulting from a transverse asymmetry of the index profile. Furthermore, to improve the accuracy of the calculations of the effective index and the form birefringence, we used the full vectorial formulation with high order polynomials of the VFEM [10].

2. The UV-induced refractive index profiles

Cladding-mode-suppression fibers (CMSFs) are manufactured with a photosensitive inner cladding to decrease the losses created by coupling to cladding modes. The parameters of the CMSF, considered in this paper, are as follows: before UV-illumination, the CMSF has a circularly symmetric step-index profile with a core radius ρ=3.05 μm and an index n_1=1.4565, a photosensitive inner cladding with a radius of σ=6.25 μm and an index n_2=1.444, and an infinite cladding with the same index n_2=1.444. In this paper, it is assumed that the photosensitive inner cladding and the fiber core have the same UV-absorption and photosensitive response. More complex photosensitive responses or gratings, leading to radially and azimuthally asymmetric index change profile could be modeled using the same numerical technique. The form birefringence of a one-side illuminated CMSF will be compared to the results obtained for one-side illuminated step-index fiber (SF) having the same core-cladding parameters but without photosensitive cladding. The form birefringence

#4024 - $15.00 US Received 16 March 2004; revised 6 April 2004; accepted 6 April 2004

of a one-side illuminated SF is also compared to the form birefringence obtained for a one-side illuminated Photosensitive Cladding Only Fiber (PCOF) with the same core-cladding parameters as the CMSF but without photosensitivity in the core. During exposure, the absorption of the UV-light incident on the side of the fiber results in an asymmetric index change profile in the photosensitive areas. For all fibers, considering illumination along the x-axis, and in the absence of saturation, the refractive index change is assumed to present an exponential decay across the photosensitive area of the fibers [3-6]:

$$\begin{cases} \delta n(x,y) = \delta n_p \exp\left[-2\alpha\left(x+\sqrt{\eta^2-y^2}\right)\right] & \text{for } \theta \le r \le \eta \\ \delta n(x,y) = 0 & \text{elsewhere} \end{cases} \quad (1)$$

where δn_p is the peak refractive index change on the side where the UV beam is incident, 2α the asymmetry coefficient, (x, y) the Cartesian coordinates in the fiber transverse plane with the origin on the fiber axis and $r=(x^2+y^2)^{1/2}$. The limits of the photosensitive region are: $\eta=\sigma$ for CMSF and PCOF, $\eta=\rho$ for SF, $\theta=0$ for CMSF and SF, and $\theta=\rho$ for PCOF. In the non-photosensitive region, the index change is equal to zero. If the index change were proportional to the absorbed intensity, the parameter α would correspond to the UV-absorption coefficient of the photosensitive region. However, we prefer to refer to α as the asymmetry coefficient because of the modeling complexity of the photosensitive response, which depends nonlinearly on the exposure intensity and time [11]. Figure 1 shows the index profiles in the SF, CMSF and PCOF for $2\alpha=0.2$ μm^{-1} and $\delta n_p=0.01$. The UV exposure is incident from x<0. The index profile along the x-axis (y=0) is also shown in Fig. 2.

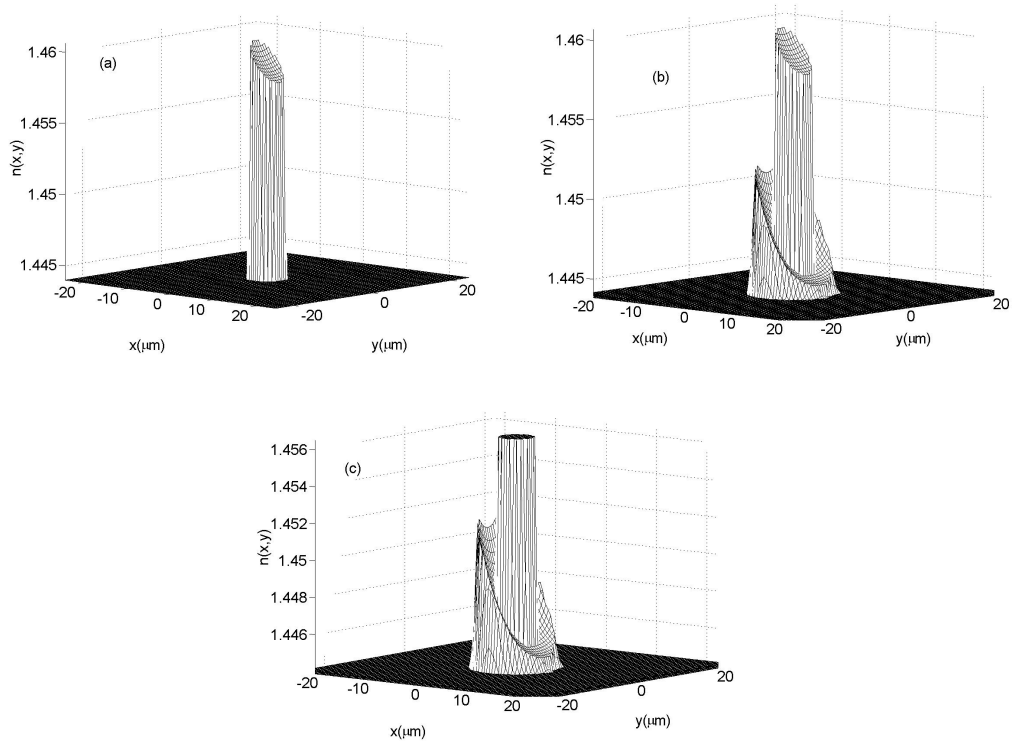

Fig. 1. The refractive index profiles for $2\alpha=0.2$ μm^{-1} and $\delta n_p=0.01$ in the (a) SF (b) CMSF and (c) PCOF.

#4024 - $15.00 US Received 16 March 2004; revised 6 April 2004; accepted 6 April 2004

3. Numerical method

In the full-vectorial approach, polarization effects are computed by solving the vectorial wave equation $\nabla\times(\nabla\times\vec{\psi})-k^2n^2(x,y)\vec{\psi}=0$ where $\vec{\psi}$ is the electric field [12]. In the Vectorial Finite Element Methods (VFEM) used in [6], the transverse field E_t is approximated by linear P_1 edge finite elements while the longitudinal component E_z is approximated by standard nodal quadratic P_2 finite elements. To increase the accuracy of the results, we use in this paper a Higher Order Vectorial Finite Element Methods (HO-VFEM) [10], where the component E_t is interpolated by P_3 edge finite elements and E_z by continuous P_4 finite elements. In order to have a high accuracy in the geometric representation, curvilinear triangles were used to approximate the core-cladding interface. The vector shape functions, especially on the curvilinear triangles, were selected in such a way that the compatibility condition is respected [10, 13]. For the unexposed SF fiber, the exact calculation of the effective index gave n_{eff}=1.450469714 at 1550 nm while the VFEM method resulted in n_{eff}=1.450463617, which represents an error of $0.6\text{x}10^{-5}$, and the HO-VFEM method resulted in n_{eff}=1.450469727, which represents an error of $1.3\text{x}10^{-8}$. In UV-exposed fibers, the birefringence calculations reported in [7] show a remarkable agreement between the HO-VFEM and the Scalar Finite Difference method with Polarization Correction. The difference between the calculated birefringence values is smaller than $1.4\text{x}10^{-7}$ for an effective index change, δn_{eff}, lowers than $5\text{x}10^{-3}$. The results presented in [7] also show that the VFEM underestimates the form birefringence. For $\delta n_{eff}=5\text{x}10^{-3}$, the difference between the form birefringence values calculated by using the VFEM and the HO-VFEM is of the order of $1\text{x}10^{-6}$ for $2\alpha=0.2\mu\text{m}^{-1}$ and $2.5\text{x}10^{-6}$ for $2\alpha=0.4\mu\text{m}^{-1}$. To improve the accuracy of the calculations, the results presented in this paper are therefore computed using HO-VFEM.

4. Results

For the index profiles shown in Fig. 1, we calculated the normalized electric fields of the modes of the one-side exposed fibers. The modes are shown in Fig. 2 where the field profiles are superposed on their respective refractive index profiles. In all three cases, the electric field has an asymmetric profile shifted towards the side of the fiber directly exposed to the UV. For the PCOF, the overlap between index perturbation and the guided mode is smaller because there is no index change in the fiber core. That explains the smaller effective index change and the smaller shift of the electric field profile observed in this type of fiber compared to the SF and CMSF.

The effective index change, $\delta n_{eff,x}$, was calculated as a function of the peak refractive index change, δn_p, for various asymmetry coefficients. The results for the CMSF and PCOF are compared to that of the SF in Fig. 3. The effective index change varies almost linearly with a weak quadratic contribution for the three illuminated fiber types. In the case of the PCOF, the curvature is larger. Furthermore, the comparison of the CMSF and SF (Fig. 3(a)) also shows that a higher peak index change is required in the CMSF to reach the same $\delta n_{eff,x}$ than in the SF. This is expected because in CMSF the peak index change first occurs in the photosensitive cladding where the overlap with the guided mode is smaller. This also explains the fact that an even higher peak index change is required in a PCOF to reach the same δn_{eff} (Fig. 3(b)), because in this case, there is no refractive index increase in the core. Similar results are obtained for the effective index changes of the mode polarized along the y-axis. We also notice that, as the asymmetry coefficient increases, higher peak index change are required to obtain the same $\delta n_{eff,x}$. In [6] it was observed that, for a given peak refractive index change, there is a value of the asymmetry coefficient (2α=0.3 to 0.4 μm^{-1}) that will maximize the photo-induced birefringence in SF.

#4024 - $15.00 US Received 16 March 2004; revised 6 April 2004; accepted 6 April 2004

The UV-induced birefringence is determined using $B=n_{eff,x}-n_{eff,y}$ where $n_{eff,x}$ and $n_{eff,y}$ are the effective indices of the fundamental mode polarized along the x- and y-axis. Notice that, in the SF case, the slow axis corresponds to the x-axis and the fast axis to the y-axis. However, in the case of PCOF and CMSF, this notion depends on the value of the index change. As is shown below, for small changes of δn_p, the x-axis is associated to the slow axis in the case of the CMSF and to the fast axis in the case of the PCOF. For higher index changes, y becomes the slow axis for the CMSF and the fast axis for the PCOF.

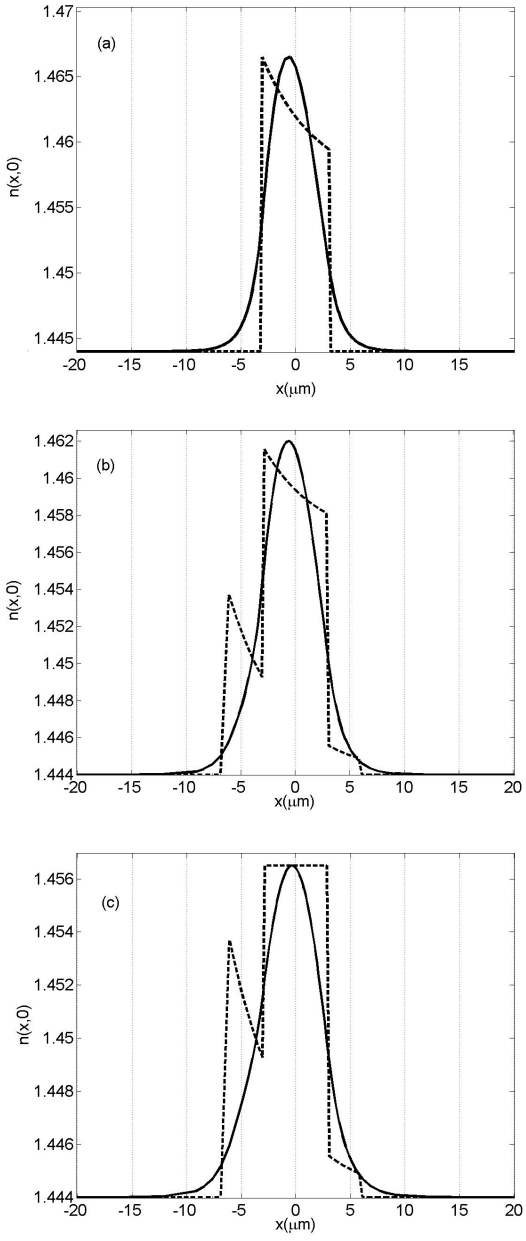

Fig. 2. The normalized electric field (solid line) superposed to the asymmetric refractive index profile (dashed line) for δn_p=0.01 and 2α=0.2 μm^{-1}. We show in (a) the SF, in (b) the CMSF and in (c) the PCOF fibers.

#4024 - $15.00 US Received 16 March 2004; revised 6 April 2004; accepted 6 April 2004

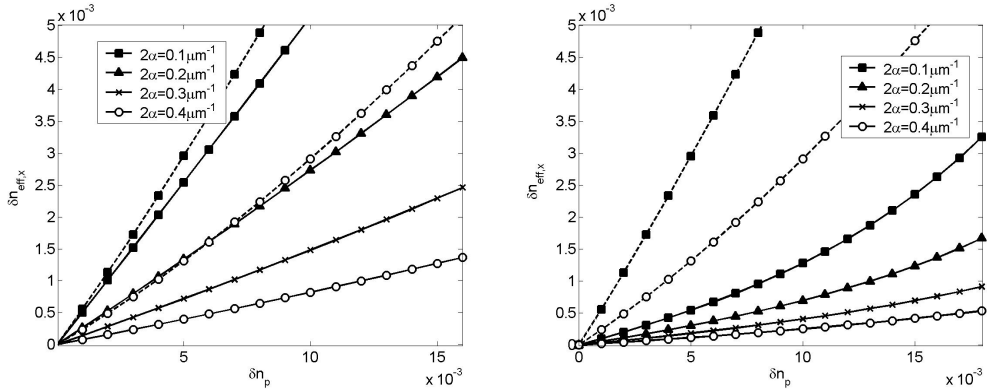

Fig. 3. The effective index change as a function of the peak refractive index change for (a) CMSF (solid lines) and SF (dashed lines) and (b) PCOF (solid lines) and SF (dashed lines).

In Fig. 4, we present the birefringence calculations for various values of 2α. The absolute value of the form birefringence of the SF shows the expected quasi-quadratic dependence on δn_{eff} [5-7]. For small values of the asymmetry coefficient ($2\alpha \leq 0.1\ \mu m^{-1}$), the birefringence of CMSF displays a similar quasi-quadratic dependence. For higher asymmetry coefficients, $0.3\ \mu m^{-1} \leq 2\alpha \leq 0.4\ \mu m^{-1}$, the birefringence reaches a maximum for $1x10^{-3} < \delta n_{eff} < 3x10^{-3}$. After this maximum, the birefringence decreases and goes through zero. The change in the birefringence sign indicates that there is a cross-over between the effective indices of the two orthogonally polarized modes: the mode polarized along the y-axis becomes associated to the slow axis and the mode polarized along the x-axis becomes associated to the fast axis. This cross-over occurs when the refractive index in the cladding reaches a value close to that of the core (Fig. 5), a situation not likely to occur in experiments because of the saturation of the photosensitive response.

In the PCOF case, the form birefringence has a quasi-quadratic shape for an asymmetry coefficient smaller than $2\alpha=0.1\mu m^{-1}$ and a parabolic shape for larger asymmetry coefficients. The form birefringence reaches an extremum for $0.5x10^{-3} < \delta n_{eff} < 1.x10^{-3}$. After this extremum, the form birefringence increases quickly and goes through zero. That reflects the same cross-over phenomenon observed in the case of the CMSF.

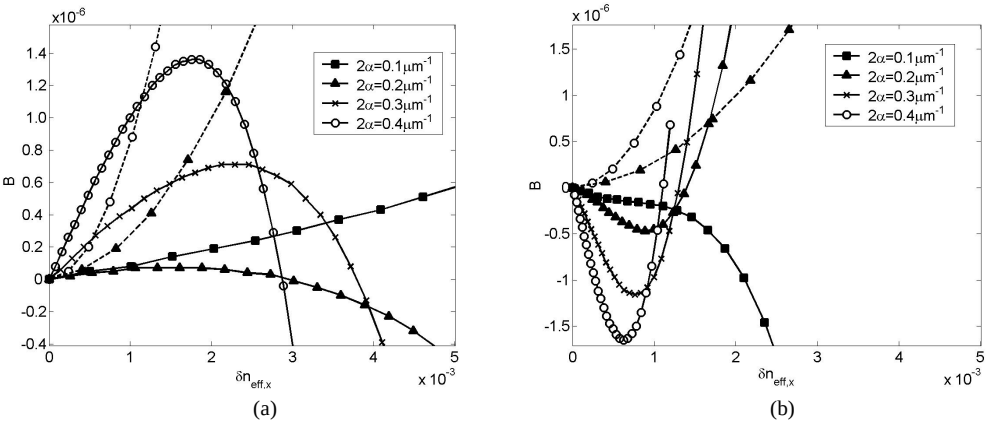

Fig. 4. The form birefringence as a function of the effective index of $\delta n_{eff,x}$ for (a) the CMSF (solid lines) and SF (dashed lines) and (b) the PCOF (solid lines) and SF (dashed lines).

#4024 - $15.00 US Received 16 March 2004; revised 6 April 2004; accepted 6 April 2004

For more usual values of effective index change where δn_{eff}<1.x10^{-3}, the birefringence in the PCOF fiber is significantly higher than the two other fiber types example. The relative value of the form birefringence in the CMSF and SF will depend on the value of the asymmetry coefficient, i.e. for 2α=0.2 μm^{-1}, the birefringence is higher in SF while, for 2α=0.4 μm^{-1} it is slightly higher in CMSF. Although the asymmetry coefficient is related to the absorption coefficient of the UV-light, the asymmetry of the refractive index change will also depend on the photosensitive response of the material including saturation effects. For example, in the case of SF fiber, an asymmetry coefficient of 2α=0.2 μm^{-1} was found to provide a good fit to the data reported in [3]. Despite the limitations of the model, it should be noted that, in all cases, the contribution of the asymmetry of the index profile to the photo-induced birefringence is typically smaller than 1.6x10^{-6} for δn_{eff}<1x10^{-3}. Although saturation is not considered in the model, it is not expected to increase the birefringence significantly [6]. In fact strong saturation will result in a more uniform index change thereby reducing the birefringence.

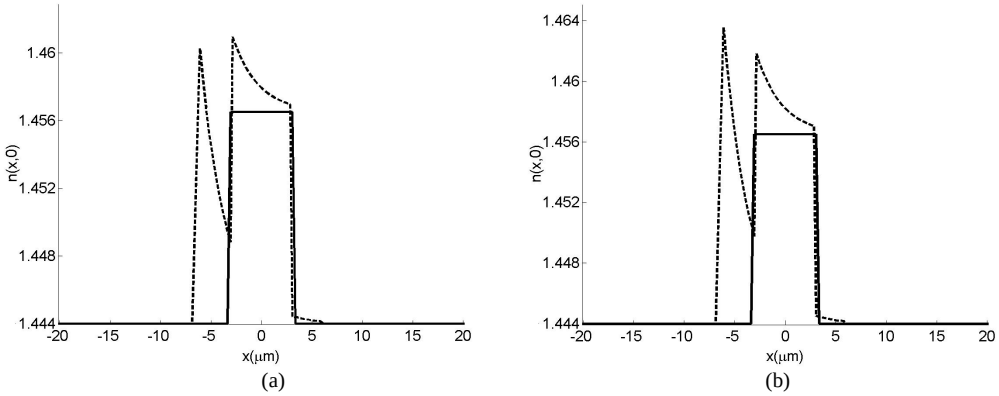

Fig. 5. The refractive index profile of the CMSF before and after illumination for (a) (2α=0.4 μm^{-1}, $\delta n_{eff,x}$=2.29x10^{-3}) and, (b) (2α=0.4 μm^{-1}, $\delta n_{eff,x}$ =2.88x10^{-3}).

Conclusion

We presented effective index and birefringence calculations using a high order vectorial finite element method in UV side-illuminated specialty fibers with a photosensitive region in the cladding. The calculations show that, in cladding mode suppression fibers and in photosensitive cladding fibers, the birefringence has a quasi-quadratic form for small asymmetry coefficients and a parabolic shape for higher values. For more usual values of effective index change, δn_{eff}<1.x10^{-3}, the form birefringence can be significantly higher in the photosensitive cladding fiber (without photosensitivity in the core) than in other fiber types. Further information about photo-induced birefringence could be obtained by developing a more complete physical model of the refractive index change that would consider saturation and anisotropy. Both these effects could be taken into account in the calculations performed using the high-order VFEM.

#4024 - $15.00 US Received 16 March 2004; revised 6 April 2004; accepted 6 April 2004